Size dependence of second-harmonic generation at the surface of microspheres

4 authors, including:

Sviatlana Viarbitskaya
University of Burgundy
22 PUBLICATIONS   **579** CITATIONS

Tony Hansson
Stockholm University
57 PUBLICATIONS   **611** CITATIONS

Size dependence of second-harmonic generation at the surface of microspheres

Sviatlana Viarbitskaya,[1] Valery Kapshai,[2] Peter van der Meulen,[1] and Tony Hansson[1,*]

[1]*Department of Physics, Stockholm University, AlbaNova University Center, SE-10691 Stockholm, Sweden*

[2]*Department of Physics, Gomel State University, BY-246019 Gomel, Belarus*

The resonance-enhanced surface second-harmonic generation (SHG) from a suspension of polystyrene microspheres was investigated as a function of particle size in a range of the order of the fundamental wavelength for two different second-harmonic-enhancing dyes—malachite green and pyridine 1. The two dyes gave the same strongly modulated pattern of the forward second-harmonic scattering efficiency. Direct comparison to the nonlinear Rayleigh-Gans-Debye (NLRGD) and nonlinear Wentzel-Kramers-Brillouin (NLWKB) model predictions showed that the NLWKB model reproduces the overall trend in the size dependence but fails with respect to the strong modulations. The standard NLRGD model was found to fail altogether in the present particle size range, which was well beyond the observed upper particle size for which the NLRGD and NLWKB models give comparable results. A generalization of the NLRGD model to allow for dispersion and to use the particle refractive indices instead of those of the surrounding medium extended its applicability range by almost an order of magnitude in particle size. There is a pronounced maximal SHG efficiency for particles with a radius that is close to the fundamental wavelength inside the particle. The optically soft particle approximation is inadequate to describe the SHG in this particle size range, as refraction and reflection of the waves at the particle surface have a decisive influence. Dispersion of the media plays a negligible role for particle sizes up to about twice the optimal one for SHG.

I. INTRODUCTION

Second-harmonic generation (SHG) at the surface of small centrosymmetric particles was first demonstrated about a decade ago [1–3]. Since then it has been employed to probe numerous physical and chemical processes occurring at the surfaces of such particles and its application to colloids provides complementary or unique tools in medicine and technology [4,5]. Examples of these uses include the characterization of molecular adsorption on polymer beads as well as clay and carbon black particle surfaces [6–8], emulsions and sprays [6,9], and biological vesicles [10]. Moreover, SHG was used to observe molecular transport across a biological membrane [10–12] and was found to be sensitive to the membrane potential of individual cells [13]. The most recent advances include the observation of SHG from single spheres in solution [14], complementing the earlier demonstration for a sphere fixed on a substrate [15], the development of a theory for the implementation of whispering gallery modes [16], as well as the observation of the large SHG enhancement due to covalent bonding of the nonlinear molecules to the surface of the dielectric spheres in colloidal crystalline arrays with photonic crystal properties [17].

The practical interest of SHG from small particles has spurred a growing number of investigations on the related fundamental physical phenomena [4,5]. For surface-related SHG, the exploration has been restricted mainly to spherical nanoparticles and clusters for which the size parameter $k_m^\omega a \ll 1$, with k_m^ω denoting the incident wave-vector magnitude in the surrounding medium and a the particle radius. In this Rayleigh scattering regime, the studied fundamental physical properties are the particle size and shape effects [18–21], the

particle concentration dependence [22,23], the polarization dependence, and the angular distribution of second-harmonic (SH) light [18,20–22,24–30]. It was shown that the total SH scattering intensity per particle scales monotonically as $(k_m^\omega a)^6$ [26].

The few studies dealing with microspheres (i.e., $k_m^\omega a \sim 1$) [14,21,24,25,27,30], have revealed a considerably more complex dependence on the particle size. The angular distribution of SH light changes dramatically with $k_m^\omega a$ [21,25] and the overall SHG increases less rapidly than in the Rayleigh range [14]. This is in accordance with calculations based on full nonlinear Mie scattering theory [18,21], which indicate that the total SH scattering intensity in this range develops an oscillatory variation with $k_m^\omega a$. Arguably, however, the employed boundary conditions at the surface of the sphere in these calculations are not quite adequate for systems with resonance enhancement from an adsorbate layer, in which case a polarization sheet model [26] seems more appropriate. So far, no applications of the polarization sheet model to systems of the kind in the present experimental study have been published. However, the two different treatments of the particle boundary region were found to yield significantly different SH scattering properties of small metallic particles [18,26], which means that one could suspect qualitatively similar deviations for adsorbate-enhanced optical SHG from dielectric microspheres.

In view of the prevailing uncertainty adhering to the treatment of the boundary layer in the rigorous nonlinear Mie scattering calculations, we resort here to the significantly simpler nonlinear versions of the Wentzel-Kramers-Brillouin (NLWKB) [27] and Rayleigh-Gans-Debye (NLRGD) models [22,24–27,29,30]. The frequently employed NLRGD model was found to reproduce measured SH polarization properties, angular distributions, and size dependence for nanoparticles with $k_m^\omega a \ll 1$ [28,29], and it has been suggested [25] that

the NLRGD model correctly describes these properties for microparticles as well. Despite the apparent success [25], the validity of the RGD approximation in the latter size range can be questioned, as it is inadequate already for *linear* Mie scattering [31]. For particles of this size, NLWKB theory [27] is appropriate. Its applicability, however, could be expected to rely on the refractive indices of the medium and the particle not being too different [32].

Here we address the issue of the size dependence of optical SHG at the particle surface and the validity of the NLRGD, in a generalized form to allow for a dispersive medium, and NLWKB theories for $k_m^\omega a \geqslant 1$. For this purpose, micron-sized polystyrene (PS) spheres in an aqueous solution of organic dye were chosen. To get an indication of the relative importance of the geometric versus molecular properties for the SHG efficiency, we employed two dyes to effect surface SHG resonance enhancement: the malachite green (MG) molecule, commonly used in the present context [1–8,10,23,24,28,29], and the previously not used pyridine 1 (Pyr1) dye, also known as LDS698. For a fundamental wavelength of 850 nm, we report an experimental observation of strong modulation in the total scattered intensity for particles with $0.45 < a < 1.5$ μm or, correspondingly, $4.3 < k_m^\omega a < 14.2$. Moreover, the size variation, within experimental uncertainty, is the same for both adsorbed dyes, which indicates that the size dependence is quite insensitive to the particular properties of the adsorbate and thus the geometric variation is the decisive condition. We derive an analytic expression for the total scattering intensity within the generalized NLRGD model and show that neither it nor the NLWKB theory reproduces the measured oscillations which were predicted qualitatively in full nonlinear Mie scattering calculations [21]. Nevertheless, the NLWKB model does reproduce the overall trends in the size dependence, whereas the generalized NLRGD theory does not.

The outline of the paper is as follows. In Sec. II we derive a generalized NLRGD expression for the scattered SH field, allowing for a dispersive medium and choice of reference for the refractive indices, and relate it to those of the standard NLRGD and the NLWKB models. The experimental setup, sample preparation, and signal extraction are then detailed in Sec. III. The chemical and physical properties of the two dye adsorbate layers and the factors influencing them are established in Sec. IV. The results of the calculations and experiments then are shown in Sec. V and discussed in Sec. VI. Finally, the main conclusions of our work are summarized in Sec. VII.

II. THEORETICAL

Consider a plane wave of angular frequency ω incident on a spherical particle with a SHG enhancing homogeneous layer of molecules adsorbed on its surface. The optical properties of the particle (p) and its surrounding medium (m) are taken to be characterized by the real refractive indices n_p^ω and n_m^ω for the incident light and $n_p^{2\omega}$ and $n_m^{2\omega}$ at the SH frequency. In the present context, it turns out, the relevant quantity at each frequency is the *relative refractive index*

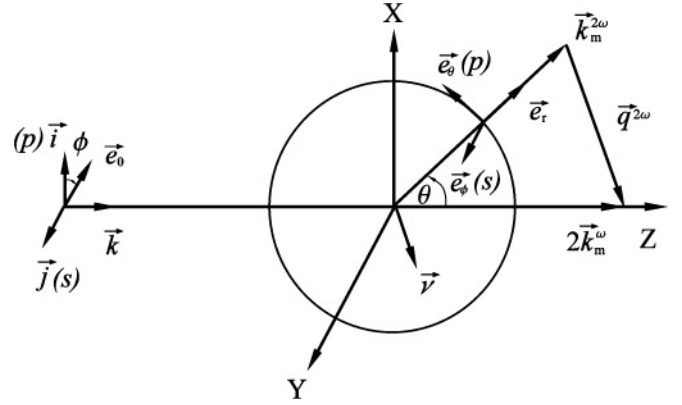$$\eta^i = n_p^i / n_m^i, \quad i = \omega, 2\omega. \tag{1}$$

FIG. 1. Cartesian (X,Y,Z) and spherical (r,θ,ϕ) coordinate systems and vectors defining the SH scattering geometry. See text for details.

We assume that SHG occurs neither in the bulk of the particle nor in the surrounding medium.

The coordinate systems and vectors used to describe the SH scattering process are shown in Fig. 1. A right-handed laboratory Cartesian coordinate system (X,Y,Z) with the corresponding basis vector set $\{\vec{i}, \vec{j}, \vec{k}\}$ is placed with its origin at the particle center. The wave vector $\vec{k}_m^\omega$ of the incoming field dependent on position $\vec{r}$,

$$\vec{E}_0^\omega(\vec{r}) = \vec{e}_0 E_0^\omega e^{i\vec{k}_m^\omega \cdot \vec{r}}, \tag{2}$$

is taken to define the Z axis. The X axis is taken to lie in the scattering plane spanned by the Z axis and a particular direction of SH light scattering conveniently described in a spherical coordinate system (r,θ,ϕ) with basis vectors $\{\vec{e}_r, \vec{e}_\theta, \vec{e}_\phi\}$, as indicated in the figure. Thus, we can write the incoming field polarization vector as $\vec{e}_0 = \cos\phi \, \vec{i} - \sin\phi \, \vec{j}$, where p and s components correspond to those of $\vec{i}$ and $\vec{j}$, respectively. Similarly, the scattered SH wave far away from the particle is characterized by the wave vector $\vec{k}_m^{2\omega} = k_m^{2\omega}\vec{e}_r$ which, by definition, lies in the XZ plane for any direction of $\vec{e}_0$. Its polarization vector can be decomposed into an s component parallel to $\vec{e}_\phi$ and a p component in the direction of $\vec{e}_\theta$. Finally, we define the *SH scattering vector* $\vec{q}^{\,2\omega} = 2\vec{k}_m^\omega - \vec{k}_m^{2\omega} = q^{2\omega}\vec{v}$; its direction is given by the unit vector $\vec{v}$.

The scattered SH field $\vec{E}_{sc}^{2\omega}(\vec{r})$ originates in the polarization $\vec{P}^{2\omega}(\vec{r}') = \epsilon_0 \chi^{(2)}(\vec{r}') \vec{E}_{inc}^\omega(\vec{r}') \vec{E}_{inc}^\omega(\vec{r}')$ induced by the incident electric field $\vec{E}_{inc}^\omega(\vec{r}')$ and mediated by the second-order susceptibility tensor $\chi^{(2)}(\vec{r}')$ multiplied by the vacuum permittivity ϵ_0. The incident field $\vec{E}_{inc}^\omega(\vec{r}')$ is the incoming field $\vec{E}_0^\omega(\vec{r}')$ modified, in general, by propagation through the particle. Only the adsorbate layer is assumed to contribute to the SHG. Accordingly, we take $\chi^{(2)}(\vec{r}')$ to be of the form $\chi_s^{(2)}(\theta',\phi')\delta(r' - a)$, where $\chi_s^{(2)}(\theta',\phi')$ is the second-order surface susceptibility tensor and $\delta(r' - a)$ is a Dirac delta function where $r' = |\vec{r}'|$ and a is the particle radius. The $\chi_s^{(2)}(\theta',\phi')$ term is related to the molecular hyperpolarizability $\beta^{(2)}$ by spatial averaging over the orientations of adsorbed molecules [33]. Here we assume that the homogeneous adsorbate layer possesses either $4mm$, $6mm$, or ∞mm local symmetry. For SHG this means that there are only three nonvanishing and independent elements of $\chi_s^{(2)}$,

namely, $\chi^{(2)}_{\perp\perp\perp}$, $\chi^{(2)}_{\perp\|\|}$, and $\chi^{(2)}_{\|\perp\|} = \chi^{(2)}_{\|\|\perp}$, where $\perp$ and $\|$ refer to the local directions perpendicular and parallel to the surface, respectively [34]. Note that from the form of $\chi^{(2)}(\vec{r}')$ it follows that only the fundamental field at the particle surface $\vec{E}^\omega_s(\vec{r}')$ is relevant; that is, in the expression for $\vec{P}^{2\omega}(\vec{r}')$ we can make the substitution $\vec{E}^\omega_{\text{inc}}(\vec{r}') \rightarrow \vec{E}^\omega_s(\vec{r}')$.

The differential SH power radiated into the direction $\vec{e}_r$ is obtained as

$$\frac{dW^{2\omega}(\theta,\phi)}{d\Omega} = \frac{1}{2}\sqrt{\frac{\epsilon^{2\omega}_{\text{m}}}{\mu}} r^2 \left| \vec{E}^{2\omega}_{\text{sc}}(\vec{r}) \right|^2, \qquad (3)$$

in which $\epsilon^{2\omega}_{\text{m}}$ is the dielectric function of the medium at the SH frequency and μ is the corresponding magnetic permeability. Consequently, the integrated SH power in a finite solid angle Ω is

$$W^{2\omega}_\Omega = \int_\Omega d\Omega' \frac{dW^{2\omega}(\theta',\phi')}{d\Omega'}. \qquad (4)$$

For comparison between calculated and measured signals, we introduce a *fractional SH scattering efficiency* into the solid angle Ω,

$$Q^{2\omega}_\Omega = \frac{1}{4\pi} \sqrt{\frac{\mu}{\epsilon^{2\omega}_{\text{m}}}} \frac{W^{2\omega}_\Omega}{a^2 \left(W^\omega_0 / A \right)^2}, \qquad (5)$$

where W^ω_0 / A is the average intensity (i.e., power per unit area) for an incoming beam of cross section A. By definition, then, $Q^{2\omega}_\Omega$ is independent of the incident intensity and the surrounding particle medium.

A. Generalized NLRGD approximation

The simplest model to be treated in detail here is NLRGD. In the spirit of the linear RGD approximation [31,35], the propagations of the incident and scattered fields are taken to be unperturbed by the presence of the particle. In its usual formulation, dispersion in the materials is ignored so that one can introduce a frequency-independent relative refractive index η. The wave vectors, likewise, do not depend on the medium and the magnitudes can be replaced by $k^{2\omega} = 2k^\omega$. These approximations taken together lead to the set of validity conditions

$$\{|\eta - 1|, |\rho|, |\zeta - 1|\} \ll 1, \qquad (6)$$

where $\rho = 4k^\omega a(\eta - 1)$ and $\zeta = n^{2\omega}/n^\omega$. The analytical expression for $\vec{E}^{2\omega}_{\text{sc}}(\vec{r})$ obtainable under these conditions has been discussed by several authors [26,27,29,30]. Note, however, that these formulations differ from each other in different and nontrivial ways, which we return to below. Before that, we derive an analytical expression for $\vec{E}^{2\omega}_{\text{sc}}(\vec{r})$ within a *generalized* NLRGD (gNLRGD) theory. For this purpose, we retain the basic RGD approximation for the incident and the SH fields but relax the restriction on the zero dispersion within the media; that is, we allow $\zeta \neq 1$. The driving field at the particle surface is $\vec{E}^\omega_s(\vec{r}') = \vec{E}^\omega_0(\vec{r}')$ in this approximation. This allows us to use an integral equation formulation analogous to the linear scattering case [36]:

$$\vec{E}^{2\omega}_{\text{sc}}(\vec{r}) = \frac{1}{4\pi \epsilon^{2\omega}} \vec{\nabla} \times \vec{\nabla} \times \int d^3 r' \frac{e^{ik^{2\omega}|\vec{r}-\vec{r}'|}}{|\vec{r}-\vec{r}'|} \vec{P}^{2\omega}(\vec{r}'). \qquad (7)$$

Rewriting this in terms of the SH scattering vector $\vec{q}^{\,2\omega}$ yields, for the Cartesian components of the scattered SH field at a large distance from the particle,

$$E^{2\omega}_{\text{sc},i}(\vec{r}) = \frac{1}{4\pi} \left(\frac{2\omega}{c} \right)^2 \frac{e^{ik^{2\omega}r}}{r} \left(E^\omega_0 \right)^2 a^2 (\delta_{ij} - e_{r,i}e_{r,j})$$
$$\times \int_{4\pi} d\Omega' e^{i\vec{q}^{\,2\omega}\cdot\vec{R}'} \chi^{(2)}_{s,jkl}(\theta',\phi') e_{0,k} e_{0,l}, \qquad (8)$$

where $\vec{R}' = a\vec{e}_r{}'$ is a point on the particle surface, δ_{ij} is the Kronecker delta, and the Einstein summation convention is implied. The difference from the simplest NLRGD theory enters here through the SH scattering vector, which by our generalization is given by

$$\vec{q}^{\,2\omega} = -2k^\omega[\zeta \sin\theta \vec{i} + (\zeta \cos\theta - 1)\vec{k}], \qquad (9)$$

for which $q^{2\omega} = 2k^\omega \sqrt{1 + \zeta^2 - 2\zeta \cos\theta}$. The corresponding NLRGD expression is easily obtained by setting $\zeta = 1$; however, this is not necessary in order to obtain an analytical solution of the integral in (8). To this end, we re-express the surface susceptibility in the form

$$\chi^{(2)}_{s,ijk} = \chi^{(2)}_1 e_{r,i}e_{r,j}e_{r,k} + \chi^{(2)}_2 e_{r,i}\delta_{jk} + \chi^{(2)}_3 (e_{r,j}\delta_{ik} + e_{r,k}\delta_{ij}), \qquad (10)$$

where $\chi^{(2)}_1 = \chi^{(2)}_{\perp\perp\perp} - \chi^{(2)}_{\perp\|\|} - 2\chi^{(2)}_{\|\|\perp}$, $\chi^{(2)}_2 = \chi^{(2)}_{\perp\|\|}$, and $\chi^{(2)}_3 = \chi^{(2)}_{\|\|\perp}$. Then the scattered SH field (8) can be written in terms of the components of $\vec{v} = \vec{q}^{\,2\omega}/q^{2\omega}$ and $v_0 = \vec{v} \cdot \vec{e}_0$ as

$$E^{2\omega}_{\text{sc},i}(\vec{r}) = \frac{i}{4\pi} \left(\frac{2\omega}{c} \right)^2 \frac{e^{ik^{2\omega}r}}{r} \left(E^\omega_0 \right)^2 a^2 (\delta_{ij} - e_{r,i}e_{r,j})$$
$$\times \left(\chi^{(2)}_1 \left\{ (v_j + 2e_{0,j}v_0) F_2(q^{2\omega}a) \right. \right.$$
$$\left. - v_j v^2_0 [3F_2(q^{2\omega}a) - F^{(3)}(q^{2\omega}a)] \right\}$$
$$\left. - \chi^{(2)}_2 v_j F^{(1)}(q^{2\omega}a) - 2\chi^{(2)}_3 e_{0,j}v_0 F^{(1)}(q^{2\omega}a) \right) \quad (11)$$

through the functions $F_2(x) = F^{(2)}(x)/x - F^{(1)}(x)/x^2$ and $F^{(\beta)}(x) = 4\pi d^\beta j_0(x)/dx^\beta$, where $j_0(x)$ is a spherical Bessel function of the first kind [37]. This is our analytical representation of the scattered SH field within the gNLRGD model.

As noted in connection with (9), the gNLRGD field (11) reduces to the standard NLRGD one if $n^{2\omega} \rightarrow n^\omega$, and it is at this point interesting to compare with previous and differing formulations for this limit. Our SH field then is consistent with that of de Beer and Roke [30] in the limit of SHG. It is similar to that of Dadap *et al.* [26], except that their field misses a factor $1/(q^{2\omega}a)$ without which the total SH intensity does not follow the expected $(k^\omega_{\text{m}}a)^6$ scaling in the Rayleigh scattering limit. Moreover, their SH scattering vector lacks the medium dependence displayed in expression (9). Compared to the NLRGD field in [29] there are discrepancies with respect to the angular distributions, whereas the angular distribution in [27] is consistent with the one obtained here. The two restricted NLRGD expressions by Yang *et al.* [25] and Martorell *et al.* [24] are in full compliance with the appropriate limit of the gNLRGD formulation presented herein.

B. NLWKB approximation

The NLWKB theory [27] partially takes into account the effects of differences in the refractive indices of the incident and scattered waves in the particle and those of the surrounding medium. Namely, each wave is assumed to propagate without refraction at the particle-medium boundary, whereas the difference in wavenumber in the particle and in the surrounding medium is accounted for. We can then write the modified incident field acting on the surface of the sphere as

$$\vec{E}_s^\omega(\vec{r}') = \frac{2}{\eta^\omega + 1} \vec{E}_0^\omega(\vec{r}') e^{i(\eta^\omega - 1)(\vec{k}_m^\omega \cdot \vec{r}' + |\vec{k}_m^\omega \cdot \vec{r}'|)}. \tag{12}$$

This field is the same as in [27] but modified by the scaling factor $2/(\eta^\omega + 1)$. The latter represents the transmission factor for a plane wave incident normally on a medium with refractive index n_p^ω from a medium with refractive index n_m^ω [32,35]. We introduce this factor in analogy to the linear WKB approximation of Klett *et al.* [32], where it was used for a better estimate of the internal field in the particle in order to correct the scaling of the extinction. Using this factor also implies that we must assume the driving field for SH polarization at the surface of the particle to be the interior field of the particle, which agrees with the literature [21,26].

Inserting this field into (7) and making a similar phase correction to the scattered SH field [27], the *i*th component of the far scattered SH field is obtained as

$$E_{sc,i}^{2\omega}(\vec{r})$$
$$= \frac{1}{4\pi} \left(\frac{2\omega}{c}\right)^2 \frac{e^{ik_m^{2\omega} r}}{r} \left(\frac{2}{\eta^\omega + 1}\right)^2 \left(E_0^\omega\right)^2 a^2 (\delta_{ij} - e_{r,i} e_{r,j})$$
$$\times \int_{4\pi} d\Omega' e^{i\vec{q}^{\,2\omega} \cdot \vec{R}' + i(\eta^{2\omega} - 1)(-\vec{k}_m^{2\omega} \cdot \vec{R}' + |\vec{k}_m^{2\omega} \cdot \vec{R}'|)}$$
$$\times e^{2i(\eta^\omega - 1)(\vec{k}_m^\omega \cdot \vec{R}' + |\vec{k}_m^\omega \cdot \vec{R}'|)} \chi_{s,jkl}^{(2)}(\theta', \phi') e_{0,k} e_{0,l} \tag{13}$$

for which no analytical solution to the integral was found. As required, this field reduces to the gNLRGD one in the limit $\{\eta^\omega, \eta^{2\omega}\} \to 1$. This limit is ambiguous, however, as it can be reached by either $n_p^i \to n_m^i$ for both of the frequencies or $n_m^i \to n_p^i$ in the reverse direction, where the first case is the one consistent with the standard NLRGD formulation. This indicates a further generalization of the latter theory, which we discuss in more detail later.

III. EXPERIMENTAL

A. Apparatus and samples

A schematic drawing of the apparatus used in our experiment is found in Fig. 2. A femtosecond Ti:sapphire laser (Tsunami, Spectra Physics) provided pulses at about 850 nm with a repetition rate of 82 MHz and averaged beam power of 0.7 W and a pulse duration of 120 fs. The linearly polarized laser beam was focused by a lens ($f = 7.4$ cm) into a fused silica cuvette with 2 mm sample thickness. Generated SH light was collected by an aspheric lens ($f = 3.7$ cm) and focused into a spectrometer (H-20 VIS, Jobin Yvon) by a combination of a plano-convex and a meniscus lens, each with $f = 40$ cm. The diameter of all lenses after the sample was
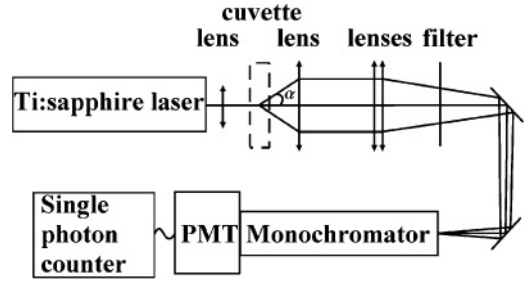

FIG. 2. Schematic experiment setup. The Ti:sapphire laser provided linearly polarized 120-fs pulses at 850 nm with a repetition rate of 82 MHz and averaged beam power of 0.7 W. The polar angle α defining the effective solid angle of detection Ω_{exp} in the 2-mm cuvette was $25°$. PMT, photo multiplier tube. See text for further details.

50 mm. A 3-mm-thick BG28 glass filter (Schott) was used to suppress the background from fundamental light entering the spectrometer. The effective collection solid angle Ω_{exp} in the liquid was measured to be confined to the polar angle $\alpha \approx 25°$. Single-photon counting was performed by means of a photomultiplier tube (PMT) (R4220P, Hamamatsu) connected to a dual-channel gated photon counter (SR400, Standford Research Systems).

Undyed plain PS microspheres (Polysciences and Bangs Laboratories) with a mean diameter in the range of 0.87 to 2.88 μm were used, which corresponds to $4.3 \leqslant k_m^\omega a \leqslant 14.2$. The size distribution was assumed to be the same as stated by the manufacturer based on dynamic light scattering experiments for $a < 1.3$ μm and following the Coulter principle otherwise [38]. The stated standard deviations in size vary from 0.3% to 23%. The undiluted PS samples in several cases contained a specified concentration, 3.5 mM, of sodium dodecyl sulfate (SDS) surfactant. Unfortunately, this information was not available for all samples, but the SDS concentration would also be expected to be similar in these cases. The samples were not washed to remove SDS, but rather, when it proved to be important (i.e., for MG solutions), SDS (10% in 18 MΩ water, Sigma-Aldrich) was added in large excess to guarantee stable adsorption conditions [39,40] (see also Sec. IV). The overall spectral resolution in the detection was about 10 nm at the SH wavelength.

Aqueous dye solutions were prepared by dissolving MG hydrochloride (80%–85% purity, Sigma-Aldrich) or Pyr1 powder (unknown purity, Radiant Laser Dyes) in deionized water and used without further purification. The PS-dye suspensions were quickly mixed without extensive shaking. The particle concentration was chosen low enough to avoid turbidity effects [5,6]; that is, depending on particle size, the order of magnitude of the polystyrene particle concentration ([PS]) was 10^6 to 10^7 ml^{-1}. Typical dye concentrations were 30–50 μM and for MG experiments [SDS] $\sim$ 1 mM, whereas with Pyr1 the [SDS] was of the order of 1 μM.

All experiments were done at room temperature and during their course no evidence of degradation of the samples was seen. There were reversible changes in the SHG on the time scale of tens of seconds, however, that we attributed to particle trapping in the laser focus.

B. Signal extraction and normalization

The measured quantity of interest is the SH signal arising from the adsorbate layer on the PS particles, $S_{\text{SHG}}^{2\omega}$. The size dependence of this signal is converted to a relative fractional SH scattering efficiency [cf. (5)], by

$$Q_{\text{exp}}^{2\omega} = \frac{S_{\text{SHG}}^{2\omega}}{a^2 \left(W_0^\omega / A \right)^2 [\text{PS}]}. \tag{14}$$

However, in general the measured signal at the SH frequency, $S_{\text{det}}^{2\omega}$, contains contributions from several sources. The significant ones here are SHG at the particle surface, hyper Rayleigh scattering (HRS), and two-photon induced fluorescence (TPF). Including background scattering from various parts of the apparatus and the PS particles, $S_{\text{app}}^{2\omega}$, we can extract the desired $S_{\text{SHG}}^{2\omega}$ from the measured signal as

$$S_{\text{SHG}}^{2\omega} = S_{\text{det}}^{2\omega} - S_{\text{HRS}}^{2\omega} - S_{\text{TPF}}^{2\omega} - S_{\text{app}}^{2\omega}, \tag{15}$$

where $S_{\text{HRS}}^{2\omega}$ and $S_{\text{TPF}}^{2\omega}$ are obtained from the dye solutions without particles and $S_{\text{app}}^{2\omega}$ is measured with only the PS particles in a pure water solution. This relatively simple signal extraction procedure relies on the fact that we have chosen to work with low enough [PS] to avoid turbidity effects.

For each particle size, $S_{\text{det}}^{2\omega}$ was measured for at least ten different [PS] to yield an average $Q_{\text{exp}}^{2\omega}$ with well-defined statistical uncertainty. All error limits indicated in the figures that follow correspond to two standard deviations, except where otherwise stated.

IV. MALACHITE GREEN AND PYRIDINE 1 ADSORBATES AS SH SOURCES

The surface SHG process here is resonance enhanced by adsorption of a suitable dye on the PS particle surface. Malachite green was used in the pioneering work [1–3] and ever since it has been the workhorse for studies of the fundamental properties of SHG from nano- and microparticles. Nevertheless, we find the need to briefly comment on the effect of the SDS surfactant on the SHG from malachite green adsorbates. In contrast, the pyridine 1 molecule has not been previously utilized for the present purpose. Thus, we prove in the second part of this section that the Pyr1-PS system behaves similarly to the MG-PS system with respect to SHG.

A. Malachite green

The SHG from MG-PS microparticles has been the subject of numerous studies [1–8,10,23,24,28,29] and therefore we do not discuss the signal contributions and adsorption processes in any detail other than that we verified that our signal reproduced the expected dependences on MG and PS concentrations.

Importantly, however, and previously unreported, for this dye there is a major impact of SDS surfactant [39,40] even with [SDS] as low as a few micromoles (see Fig. 3). The [SDS] dependence of the signal in Fig. 3 is typical for all particle sizes. Thus, there is an initial very steep variation below 100 μm, then a plateau extending to about 1 mM and finally a gradual monotonic decrease for even higher [SDS]. We do not find the details of this behavior essential for the present purpose, but we contend that it is consistent with a
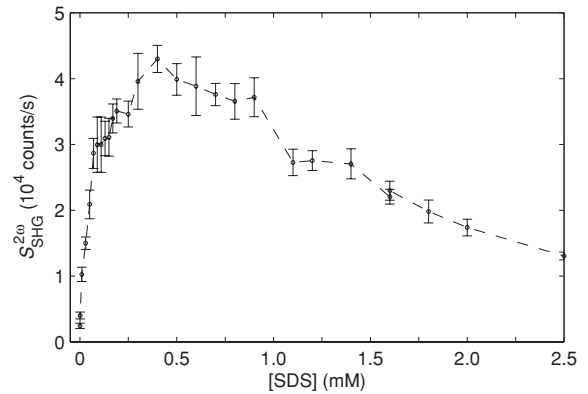

FIG. 3. Second-harmonic signal as a function of SDS concentration for a PS-MG-SDS suspension. [MG] = 30 μM, [PS] = 1.0×10^7 ml^{-1}, and $k_m^\omega a = 6.7$.

process involving coadsorption of MG and SDS on the PS surface and that this process has reached a stable equilibrium for [SDS] $\sim$ 1 mM. Moreover, the similarity of the [SDS] dependences for particles of different sizes indicates that the adsorbate layers at the plateau concentrations are equivalent.

The strong signal dependence on [SDS] in the μm range, which are typical concentrations that ensue from the dilution of the PS samples to obtain the experiment sample, potentially causes severe problems because of uncertainties in the SDS concentration. Here we avoid this problem by choosing to work in the plateau region of the [SDS] dependence for large [MG] in which the excess of added SDS is large enough to ensure that any initial SDS present in the diluted PS sample is negligible.

The PS-MG-SDS samples behaved similarly in every aspect of SHG to that previously reported for PS-MG particles. Thus, we refrain from reporting redundant data and refer the reader to the literature for details [1–8,10,23,24,28,29]; however, in view of the lack of discussion on the presence of SDS surfactant in the PS samples, we would at this stage caution against taking the previously reported adsorption mechanisms and Langmuir adsorption parameters too literally.

B. Pyridine 1

Pyridine 1 has not previously been used to investigate surface SHG from nano- or microspheres. We therefore reserve some space here to provide evidence that Pyr1 mostly behaves analogously to MG with respect to resonance enhancement of surface SHG and dye concentration dependence. However, in one important aspect it is different from MG: there is no clear dependence of the SHG on [SDS] in the micromolar range. On the other hand, the Pyr1 suspension shows evidence of aggregate formation at [SDS] > 6 μM (see below).

The absorption spectrum of Pyr1 features the S_1 transition as a broad peak at 480 nm [41–44] and the observation of resonance-enhanced SHG in this wavelength region has been reported for Pyr1 adsorbates on fused silica [45,46]. Thus, S_1 resonance-enhanced SHG might also be expected to be effective on polystyrene substrates, which we, indeed, find to be the case. For a start, Fig. 4 shows the scattered spectrum resulting from 860-nm irradiation of samples of
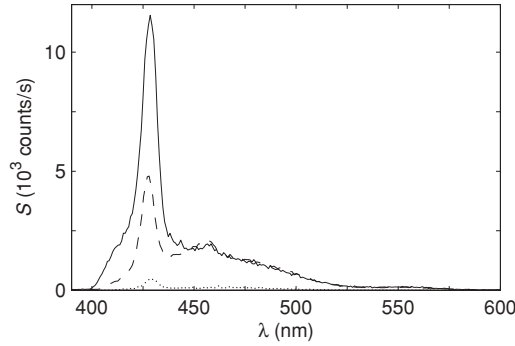
FIG. 4. Total emission S spectra for PS (dotted curve), Pyr1 (dashed curve), and PS-Pyr1 (solid curve) solutions and suspensions with $\lambda^\omega = 860$ nm. In the various cases [Pyr1] $= 50$ μM and [PS] $= 5.0 \times 10^6$ ml^{-1}, as applies, and $k_m^\omega a = 13$.

FIG. 5. Total signal at the SH wavelength for a PS-Pyr1 suspension (points) and a linear least-squares fit (line). [Pyr1] $= 50$ μM, [PS] $= 1.0 \times 10^7$ ml^{-1}, and $k_m^\omega a = 13$. The unity constants $W_1 = 1$ mW and $S_1 = 1$ s^{-1} ensure that the logarithm arguments are dimensionless.

various compositions. The curve with PS suspension in pure water illustrates the typical background signal $S_{app}^{2\omega}$ and it is not significantly different from that of pure water (not shown). There is a small contamination from Pyr1 remaining after cleansing of the cuvette, contributing about 50 counts/s at 480 nm and 200 counts/s at 430 nm. In the present case, this background signal is negligible compared to that from the aqueous Pyr1 solution without PS particles. The shape of that spectrum indicates that there is a significant $S_{HRS}^{2\omega}$, which is different from the MG solution for which HRS was below detectable levels. Connected to the HRS peak, which naturally shifts with laser wavelength, there is a structure approximately 30 nm to the red that shifts with laser wavelength as the HRS peak does. The likely mechanism behind this peak is hyper Raman scattering, which has been shown to produce such features in similar molecules [47,48]. Finally, there seems to be a small TPF contribution with a band shape similar to that of the S_1 band. This is a bit surprising, as time-resolved studies [43,44] of the S_1 relaxation of Pyr1 in other solvents have indicated a fast and efficient process that causes the main TPF to appear at around 650 nm, which was outside the detection capacity of our apparatus. To further consolidate our assignment of the peak at 430 nm to HRS, we note that this is an incoherent second-order process and as such it would be expected to scale linearly with [Pyr1] [33]. This, indeed, is what we observe for the assigned $S_{HRS}^{2\omega}$.

Upon addition of the polystyrene particles to the Pyr1 solution, there is a strong enhancement of the peak at the expected wavelength of SH light, but little else happens. Thus, the induced difference ought to be due to SHG from Pyr1 adsorbed on the PS surface. The total signal $S_{det}^{2\omega} \approx S_{SHG}^{2\omega} + S_{HRS}^{2\omega}$ should scale quadratically with the incident laser intensity, as is found to be the case from inspection of Fig. 5. Moreover, as SHG is a coherent process, for small [Pyr1] the $S_{SHG}^{2\omega}$ should scale quadratically with the surface concentration of Pyr1, provided the molecular surface density in this range is proportional to [Pyr1]. The required quadratic dependence is nicely illustrated in Fig. 6. In the same figure, it is also shown that the $S_{SHG}^{2\omega}$ as a function of [Pyr1] over a wider range varies qualitatively as in the MG system. Thus, above a certain [Pyr1], the PS surface seems to be saturated by dye molecules and the surface density of Pyr1 in this [Pyr1] range should be representative for all particle sizes.
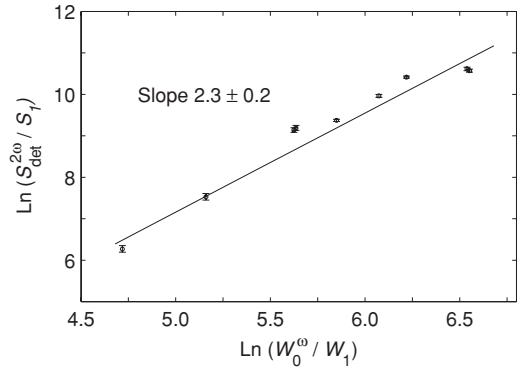
In view of the dramatic effect of the presence of low concentrations of SDS on the SHG from the MG-PS system, we also investigated this issue for the Pyr1 case. As illustrated in Fig. 7, there is no discernible correlation between the average signal and the [SDS]. There is a correlation, however, when comparing similar graphs for the various particle sizes: a consistent increase of the variance of $S_{SHG}^{2\omega}$ for [SDS] > 6 μM. Furthermore, for [SDS] in the millimolar range, there is rapid precipitation of the sample. Thus, we take the increased uncertainty in the $S_{SHG}^{2\omega}$ for [SDS] > 6 μM as an effect of the onset of aggregation of Pyr1 and SDS. This is well above the SDS concentration in our diluted PS particle samples, however, and in view of the manifested independence of $S_{SHG}^{2\omega}$ on [SDS] in this case, we expect the somewhat uncertain SDS concentrations not to cause any trouble and use the diluted PS particle samples as such.

Clearly, Pyr1 adsorbate on PS is an efficient SH source and thus is a readily available alternative to the frequently applied MG molecule to study surface SHG by nano- and microparticles. A drawback, however, is that very little is known of the nonlinear properties for Pyr1 in general [42] and the second-order ones in particular [45,46]. A comparison to closely related molecules in [49] indicates that the molecular hyperpolarizability $\beta^{(2)}$ for Pyr1 should be of a magnitude similar to that for MG [50].

V. RESULTS: SIZE DEPENDENCE OF SHG

In general, the SH scattering depends on the effective surface susceptibility $\chi_s^{(2)}$. To bring out some general features of the size dependence and their manifestation in the measured data, in Sec. V A we show calculations using the NLRGD, gNLRGD, and NLWKB models restricted to the case of a purely radial susceptibility tensor (i.e., $\chi_s^{(2)} \equiv \chi_{\perp\perp\perp}^{(2)}$). The influence of the particular form of $\chi_s^{(2)}$ within the models is then investigated by comparison of calculations for each of the three possibly nonvanishing $\chi_s^{(2)}$ components. The latter procedure is essential in order to assess the reliability of the measured size dependence, because of the above-mentioned uncertainty regarding the exact form of $\chi_s^{(2)}$ in the experiments: for Pyr1 it is unknown, whereas for MG conflicting results have been
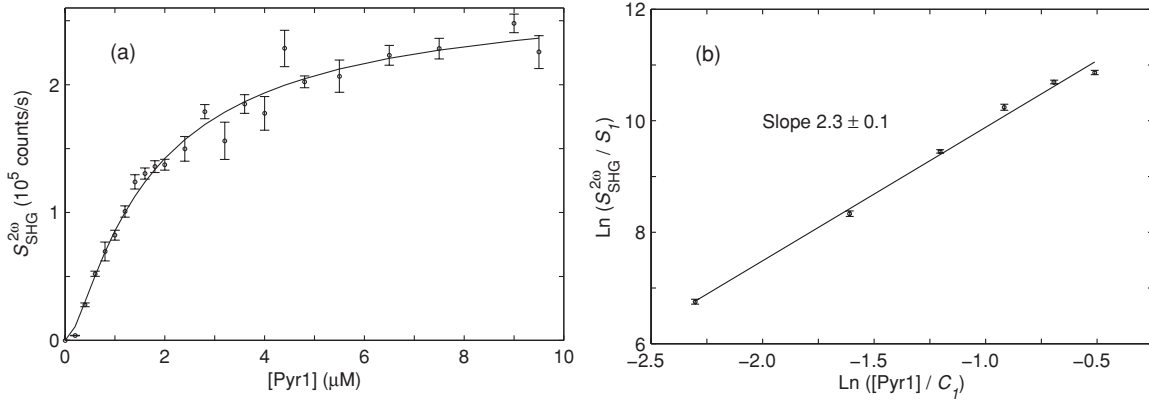
FIG. 6. SH signal (points) as a function of Pyr1 concentration for a PS-Pyr1 suspension. $[PS] = 3.0 \times 10^7$ ml^{-1} and $k_m^\omega a = 8.1$. (a) Linear graph over a range in [Pyr1] wide enough to indicate saturation behavior and a least-squares fit of the modified Langmuir model [3]. (b) Logarithmic graph in the presaturation region and a linear least-squares fit (line). The unity constants $C_1 = 1$ μM and $S_1 = 1$ s^{-1} ensure that the logarithm arguments are dimensionless.

reported [25,28]. In Sec. V B we present the measured SH size dependence for the two different adsorbates and compare to calculations.

A. Model predictions

As pointed out in connection with (13), the gNLRGD limit can be reached in two ways within the NLWKB model, corresponding to the SH scattering being governed by the refractive indices of the medium, $n_m^\omega = 1.33$ and $n_m^{2\omega} = 1.35$ [51], or the particle, $n_p^\omega = 1.58$ and $n_p^{2\omega} = 1.62$ [52]. The first case corresponds to that of the standard NLRGD theory and the second is what we refer to as particle-governed SH scattering. Below, we use an index gNLRGD$_{m/p}$ to distinguish these two limiting cases. Because of the value of ζ being very close to 1 for the present system, the gNLRGD$_m$ model yields curves that in no essential way differ from the NLRGD curves. Therefore, to avoid cluttering of the graphs we do not show the gNLRGD$_m$ curves and plot only gNLRGD$_p$ results.

The overall SHG efficiency as a function of the size parameter $k_m^\omega a$ calculated within the NLRGD, gNLRGD$_p$ and NLWKB models is shown in Fig. 8. For small size parameter values, the models predict similar behavior with the expected

a^4 scaling in the Rayleigh scattering regime [21,26]. The discrepancies remain small up to $k_m^\omega a \sim 1$, at which point the models develop qualitatively very different $k_m^\omega a$ dependences. Beyond the illustrated range up to $k_m^\omega a = 100$, the NLRGD curve increases monotonically whereas the gNLRGD$_p$ one goes through a weak maximum at $k_m^\omega a \approx 30$ and levels out at a value of 0.7 (arbitrary units) in Fig. 8. The NLWKB curve, on the other hand, indicates an oscillatory behavior with a minimum at $k_m^\omega a \approx 50$ with very low SHG efficiency and a maximum again at twice the size parameter value.

The SH angular distribution also varies with the particle size, as illustrated with graphs for a few representative $k_m^\omega a$ in Fig. 9. In the Rayleigh scattering regime at very small $k_m^\omega a$, the three models predict similar wide-angle scattering with vanishing intensity in the forward direction, as expected from [28,29]. As $k_m^\omega a$ increases, the angular distribution folds into the forward direction and develops side lobes. For $k_m^\omega a \approx 1$, the gNLRGD$_p$ and NLWKB distributions are still identical, whereas the NLRGD one is shifted to larger angles. This difference grows rapidly with the particle size, while the two former models stay in reasonable agreement up to
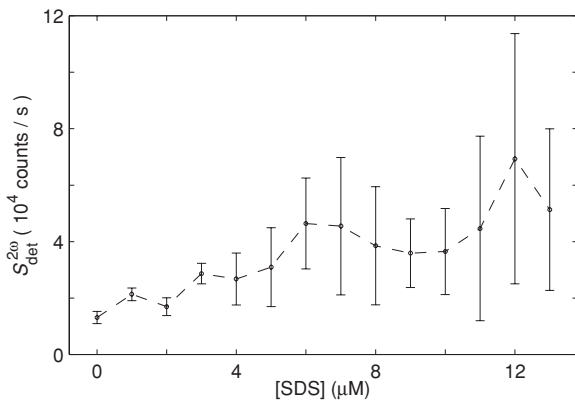

FIG. 7. Total signal at the SH wavelength as a function of SDS concentration for a PS-Pyr1-SDS suspension. $[Pyr1] = 50$ μM, $[PS] = 1.0 \times 10^7$ ml^{-1}, and $k_m^\omega a = 4.9$.
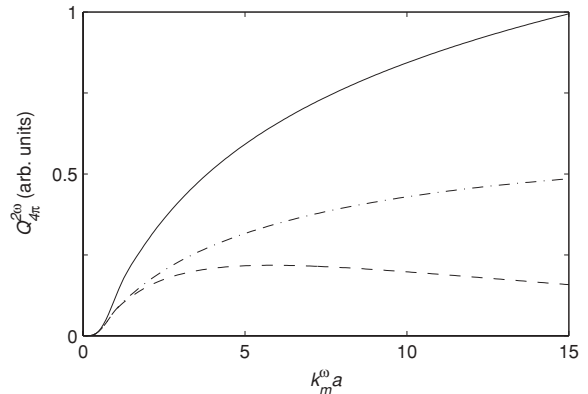

FIG. 8. Calculated total SH scattering efficiency as a function of size parameter for all three models: NLRGD (solid curve), gNLRGD$_p$ (dash-dotted curve), and NLWKB (dashed curve). $\chi_s^{(2)} = \chi_{\perp\perp\perp}^{(2)}$ in all cases.
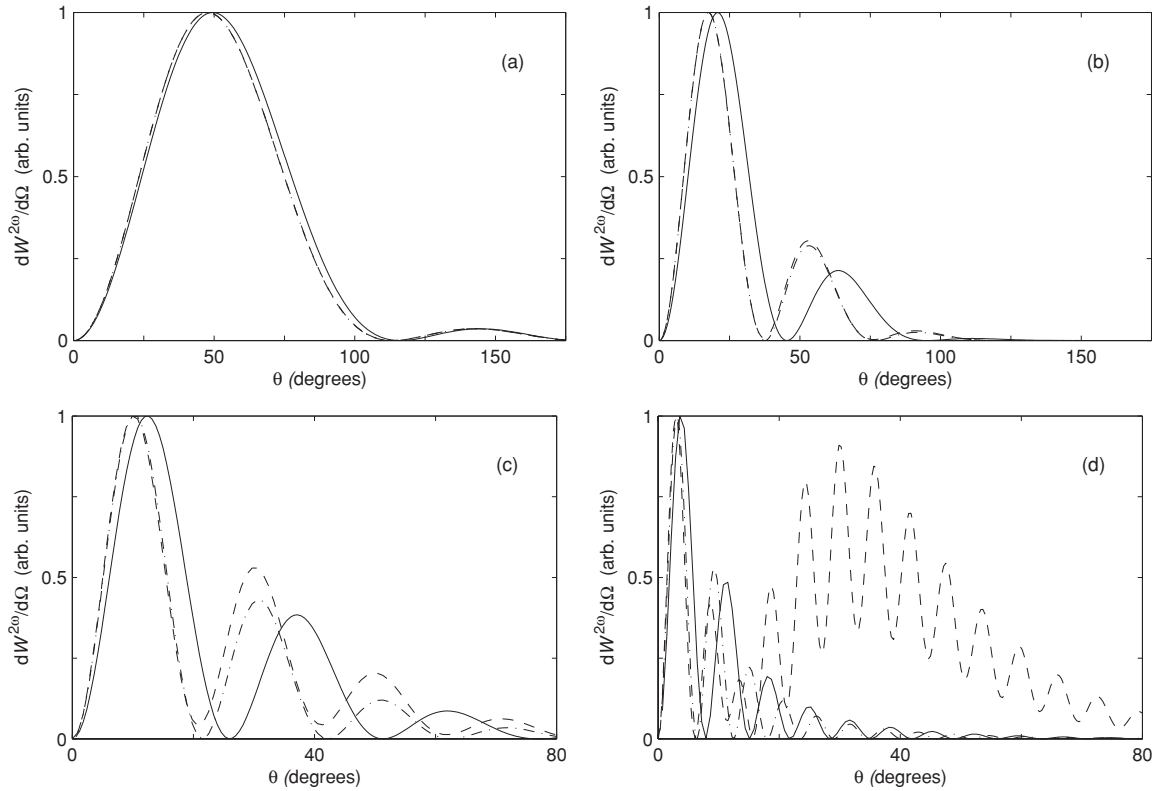
FIG. 9. Calculated SH angular distribution in p-in/p-out polarization configuration for selected particle sizes and for all three models: NLRGD (solid curve), gNLRGD$_p$ (dash-dotted curve), and NLWKB (dashed curve). Note that the gNLRGD$_p$ and NLWKB curves in (a) coincide. In all cases, $\chi_s^{(2)} = \chi_{\perp\perp\perp}^{(2)}$. The $k_m^\omega a$ values are (a) 0.49, (b) 2.5, (c) 4.3, and (d) 14.

$k_m^\omega a \approx 2.5$. At even larger $k_m^\omega a$, clear discrepancies develop as the NLRGD and gNLRGD$_p$ models produce essentially constant envelopes of the scattering pattern, whereas NLWKB exhibits a redistribution of the overall scattering intensity over a significantly wider angular range. Nevertheless, the gNLRGD$_p$ model still fits the NLWKB scattering pattern very well for small angles. In all cases, the scattering in the exact forward direction is zero, in accordance with symmetry requirements [53].

The variation in SH angular distribution has an effect on the measured SHG size dependence through the restricted solid angle of detection. This is directly reflected by the detection efficiency

$$ N = W_{\exp}^{2\omega} / W_{4\pi}^{2\omega}, \qquad (16) $$

where the detected intensity $W_{\exp}^{2\omega}$ is obtained from (4) with $\Omega = \Omega_{\exp}$, shown in Fig. 10 as a function of the size parameter. Accordingly, all three models yield very small detection efficiency in the Rayleigh scattering range in which large-angle SH scattering dominates. For small and moderately large $k_m^\omega a$, the general shape of the angular distributions in the models is quite similar and the predicted detection efficiencies remain close, but beyond 2.5 they diverge as a consequence of the aforementioned broadening of the NLWKB distribution. The strong deviation among the NLRGD and gNLRGD$_p$ models, on the one hand, and the NLWKB model, on the other hand, for large $k_m^\omega a$ is not surprising in view of the severe violation of the validity restrictions on the linear RGD size parameter in this $k_m^\omega a$ range. For smaller particles, in the presumed

validity range of the standard NLRGD formulation [25], we note that its prediction deviates significantly from that of the NLWKB already for $k_m^\omega a$ on the order of 0.1. The gNLRGD$_p$ curve remains indistinguishable from the NLWKB one up to $k_m^\omega a \approx 2.5$.

It remains to establish the sensitivity of the detected signal to the explicit form of the $\chi_s^{(2)}$ tensor. To this end, Fig. 11 shows the calculated variation of the SH scattering efficiency into the detection solid angle, $Q_{\exp}^{2\omega}$, for all three possibly
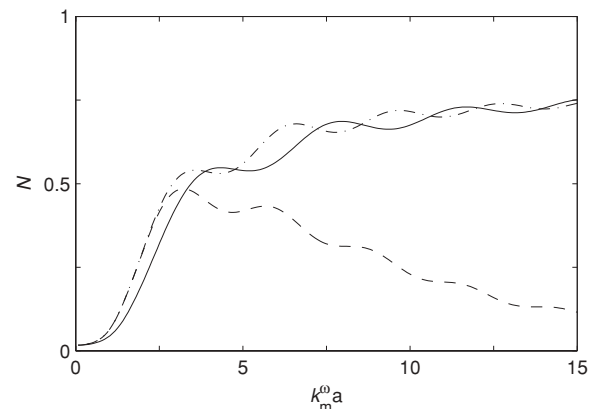

FIG. 10. Calculated SH detection efficiency as a function of size parameter for all three models: NLRGD (solid curve), gNLRGD$_p$ (dash-dotted curve), and NLWKB (dashed curve). $\chi_s^{(2)} = \chi_{\perp\perp\perp}^{(2)}$ in all cases.
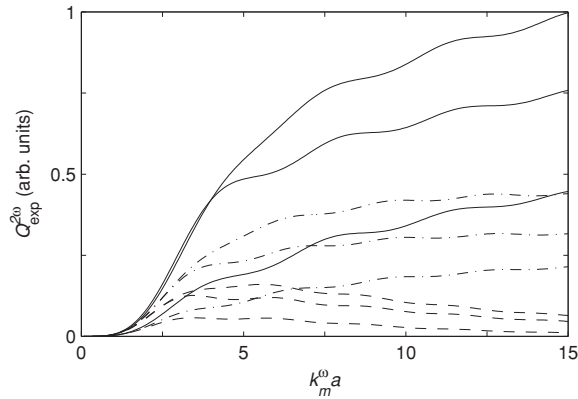
FIG. 11. Calculated fractional SH scattering efficiency in the detection solid angle for various $\chi_s^{(2)}$ components as a function of size parameter for all three models: NLRGD (solid curve), gNLRGD$_p$ (dash-dotted curve), and NLWKB (dashed curve). For each model, the three lines correspond to $\chi_s^{(2)} = \chi_{\perp\perp\perp}^{(2)}, \chi_{\perp\|\|}^{(2)}, \chi_{\|\|\perp}^{(2)}$, in order from bottom to top.

nonzero $\chi_s^{(2)}$ components. In $Q_{\exp}^{2\omega}$, both the size and the angular distribution variations are included and we see that all models predict a qualitatively similar $k_m^\omega a$ dependence of the measured partial SH scattering efficiency for all tensor components. The variation, which we see shortly from the comparison to measured data, is less than that from other effects not incorporated in the models. Accordingly, we arbitrarily choose the overall surface susceptibility to be represented by a purely radial one; that is, we take $\chi_s^{(2)} \equiv \chi_{\perp\perp\perp}^{(2)}$.

B. Measurements

The particle size dependence of the second-harmonic generation measured with both malachite green and pyridine 1 as adsorbate is shown in Fig. 12 in terms of the fractional SH scattering efficiency in the detection solid angle. The corresponding NLWKB and gNLRGD$_p$ results are also indicated together with the those of the nonlinear Mie scattering theory by Pavlyukh and Hübner [21]. In the case of MG, to ensure uniform adsorption conditions, the measurements were made at the stability plateau of the [SDS] around 1 mM (Fig. 3). It should be noted that if this precaution is not taken, the size dependence measurements yield perfectly reproducible but significantly dissimilar results to those presented here [40]. For the Pyr1 experiments, on the other hand, the requirement to avoid sample aggregation meant that the [SDS] was kept as low as possible (Sec. IV B) (i.e., on the order of 1 μM).

Allowing for the statistical and systematic uncertainties in the experiments, the two adsorbates yield very similar dependence of $Q_{\exp}^{2\omega}$ on the particle size, as shown explicitly by the shading in Fig. 12. Thus, irrespective of the expected different molecular hyperpolarizabilities—MG having a dominating $\beta_{zxx}^{(2)}$ component [54], while following the arguments in [49] we expect the $\beta_{zzz}^{(2)}$ to dominate in Pyr1—the overall properties of the adsorbate layers are similar enough with respect to SHG in the general forward direction to eliminate significant dependence on the chemical identity of the adsorbate. This finding is reassuring as it indicates that the measured variation
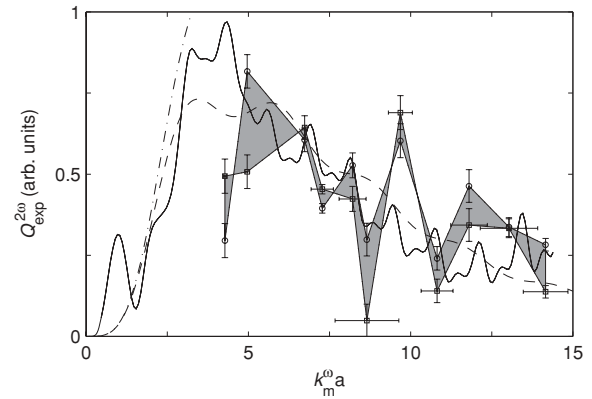

FIG. 12. Fractional SH scattering efficiency in the detection solid angle as a function of size parameter measured for both adsorbates, MG (squares) and Pyr1 (circles), and calculated for gNLRGD$_p$ (dash-dotted curve) and NLWKB (dashed curve) models and the nonlinear Mie scattering model by Pavlyukh and Hübner [21] (solid curve). The shading shows the difference between the two measured data sets. The measured data sets were normalized to each other at $k_m^\omega a = 13$. In all cases, $\chi_s^{(2)} = \chi_{\perp\perp\perp}^{(2)}$. The error bars in both directions correspond to a statistical error of one standard deviation. (Standard deviations in size vary from 0.3% to 23%.)

in $Q_{\exp}^{2\omega}$ with $k_m^\omega a$ is due to the SHG size dependence only.

Comparing the measured data to the calculated $Q_{\exp}^{2\omega}$ curves in Fig. 12, we see that the NLWKB model captures very well the overall trends in the size dependence. The RGD-based models fail altogether in this respect. All of these models yield weak oscillations due to the regular evolution of the SH angular distribution, but none is close to the strong modulation observed in the measurements. The nonlinear Mie scattering model, on the other hand, shows more pronounced modulations.

VI. DISCUSSION

The main point to be discussed here is the particle-size dependence of the SH scattering efficiency. For this purpose, the measured data are analyzed within the framework of the NLWKB model and qualitatively compared to the nonlinear Mie scattering theory by Pavlyukh and Hübner [21]. Restrictions on the applicability of the NLRGD and gNLRGD models are identified as well.

Before delving into a detailed interpretation of the SHG dependence on the particle size, we need to discuss possible influences by apparatus or chemical nature. Jen and Dai [29] observed that the SHG efficiency from a MG adsorbate layer was affected by the chemical composition of the polystyrene particle surface. That work considered particles with diameters an order of magnitude smaller, however, for which different manufacturing procedures had been used for the various particle sizes. This should not be the case for the particles used here and, indeed, measurements of MG "adsorption isotherms" for different particle sizes (not shown) could be well fitted with a single pair of modified Langmuir model parameters [39,40], indicating chemically equivalent PS surfaces. This

conclusion is further corroborated by the fact that the MG and Pyr1 adsorbates give similar measured SHG dependences on particle size. The quite different chemical structures of the two adsorbates suggest that they would respond rather dissimilarly to changes in the adsorption environment, which is observed with respect to the effect of the presence of SDS surfactant in the solution.

Evidence against apparatus-related artifacts strongly influencing the observed SHG size dependence is indirectly provided by the sensitivity of the MG-PS system to the presence of SDS in the solution. Namely, as noted in Sec. IV A, the measured size dependence, including the modulation pattern for the MG system, is very different from that in Fig. 12, unless care is taken to equalize the SDS concentration in the samples [40]. We considered a polarization bias of the spectrometer grating on the order of 10% insignificant in the present context.

Having ascertained the absence of significant experimental artifacts, we turn to our central theme of the SHG dependence on the particle size. The measured variation of $Q_{\exp}^{2\omega}$ is proportional to the *total* SH scattering efficiency $Q_{4\pi}^{2\omega}$ folded with a variation of the SH angular distribution, causing changes in the fraction of the SH light scattered into the detection solid angle. From Fig. 8 it is seen that within the NLWKB model $Q_{4\pi}^{2\omega}$ varies only marginally after a rapid increase up to $k_{\mathrm{m}}^{\omega}a \sim 1$ with further increasing $k_{\mathrm{m}}^{\omega}a$ in the displayed range. At the same time, the envelope of the SH angular distribution broadens (Fig. 9), which causes the reduction in the SH detection efficiency in Fig. 10. In the NLWKB approximation, the overall form of measured $Q_{\exp}^{2\omega}$ size dependence reflects almost entirely the variation of the envelope of the SH angular distribution. This finding opposes the prediction by Yang *et al.* [25] that the angular distribution with increasing particle size becomes increasingly confined to a narrow range in the forward scattering direction. Their reasoning, however, is based on the standard NLRGD model, which, we see from Fig. 9, fails to reproduce the SH angular distribution for $k_{\mathrm{m}}^{\omega}a$ larger than about 1.

Overall, the measured SHG size dependence follows the smooth one of the NLWKB model, but it also exhibits superimposed modulations. Clearly, the physical mechanism behind these modulations is missing in the NLWKB formulation. Thus, the modulations cannot be explained in terms of a simple phase shift due to rectilinear propagation through the particle interior of interfering 2ω waves originating from different points on the particle surface. This mechanism should be viewed as responsible for the overall size dependence, which would exhibit oscillations on a larger particle-size scale. To recover the fast modulations observed here, we must abandon the optically soft particle approximation and allow for refraction and reflection of the waves at the particle surface. These effects are included in the nonlinear Mie scattering theory by Pavlyukh and Hübner [21], and we included the results from calculations based on this theory in Fig. 12. In view of the disputable choice of boundary conditions in the present context, we only give significance to the qualitative features of the SHG size dependence. Nonetheless, overall it agrees well with the measured value and there are stronger modulations than for the NLWKB model. These modulations are due to oscillations in the total scattering SH efficiency and a concomitant large variation in the SH angular distribution

with particle size [21]. Accordingly, we attribute the observed modulations of the measured fractional SH efficiency to the same mechanism. It results from a more complex interaction of electromagnetic fields than that included in the NLWKB theory. Nevertheless, demonstrably, the NLWKB model does have the capability to predict the overall trend in the size dependence of the forward SH scattering in the particle size range studied here.

In sharp contrast to the NLWKB model, the RGD-based models do not reproduce the SHG variation with particle size at all. They are much simpler to use, however, so it is still of practical interest to briefly discuss their applicability limits. In order to quantify these limits, we consider a model to be out of range when its $Q_{4\pi}^{2\omega}$ value deviates more than 10% from that of the NLWKB model. It is clear from (6) that the nonlinear RGD approximations, if they apply at all, apply in the small-particle limit. Consistently, Figs. 8–11 show that the three analytical models give nearly identical results for the smallest particles up to $k_{\mathrm{m}}^{\omega}a \lesssim 1$, beyond which they differ increasingly. A closer look reveals that the standard NLRGD model breaks down at $k_{\mathrm{m}}^{\omega}a \approx 0.5$, whereas the gNLRGD$_{\mathrm{p}}$ model remains valid until $k_{\mathrm{m}}^{\omega}a \approx 2$. These limits are fairly less restrictive than those in (6), which may seem surprising. But in fact, for the present system, the linear RGD also works well outside the formal validity range [55]. Employing the results for the applicability limits of the linear RGD approximation from [55] to both the fundamental and the second-harmonic waves, we get a combined estimate which is identical to that we see for the NLRGD calculations.

The agreement between the results of the NLWKB, gNLRGD, and standard NLRGD theories for $k_{\mathrm{m}}^{\omega}a$ up to about 1 shows that, for SH scattering from particles in this size range, the only relevant physical parameter is the particle diameter. In the limit of a vanishing size parameter, the SH intensity increases proportionally to $(k_{\mathrm{m}}^{\omega}a)^{6}$ in all the models, while most of the SH radiation is emitted at more or less right angles to the incoming laser beam [28,29]. It should be noted that, although being a rather coarse correction of the internal particle field, the transmission factor of $2/(\eta^{\omega}+1)$ in (12) improves the agreement between the NLWKB and NLRGD models for small particles.

The choice of the particle refractive index instead of that of the surrounding medium in the gNLRGD model extends its validity range dramatically. The optical path length for the SH inside the particle is then included properly, and good agreement with the NLWKB theory suggests that for small particles this is indeed the major factor determining the outcome of the calculation. Dispersion plays only a very minor role here and is negligible for $k_{\mathrm{m}}^{\omega}a$ up to about 8. This is easily understood by observing that the differences in the refractive indices between the medium and the particle are about one order of magnitude larger than the dispersion inside the medium or inside the particle. All in all, the previously used standard NLRGD model based on the refractive indices of the surrounding medium should be abandoned and could be well replaced by the dispersionless gNLRGD$_{\mathrm{p}}$ model as the simplest analytical model for small particles.

The discrepancy between the gNLRGD$_{\mathrm{p}}$ and NLWKB models grows as $k_{\mathrm{m}}^{\omega}a$ increases beyond approximately 2, which reflects that the relative refractive indices start to play a

significant role. From Figs. 8 and 9 it can be seen that a major source of this discrepancy lies in the angular distribution. The general trend in Fig. 9 is that the NLWKB model predicts more scattering intensity than the gNLRGD$_p$ does at large angles, and for the largest particles treated here the angular distribution becomes very wide with most intensity outside our experimental collection angle. In addition, the distribution becomes quite complex with many minima and maxima. In contrast, both NLRGD and gNLRGD$_p$ indicate that for such large particles the SH radiation would be emitted in a relatively narrow cone around the forward direction. These differences in the predicted angular distribution are, of course, reflected in the detection efficiency in Fig. 10 and reinforce the already substantial differences in the total SH scattering efficiency in Fig. 8, as the two are combined to yield the substantial differences in the detected fractional SH scattering efficiency seen in Fig. 11.

It is instructive to compare the picture emerging from the present study with the often-cited simple model by Wang *et al.* [3]. These authors found that the power of the generated SH light should display an oscillatory behavior as a function of particle size, that no SH radiation should be generated for spherically symmetric particles much smaller than the wavelength of the fundamental wave, and that the output of SH light should be maximal for those particle sizes for which $\Delta k_p a = (2n + 1)\pi/2$, where $\Delta k_p = k_p^{2\omega} - 2k_p^\omega$ is the phase mismatch from propagation through the particle.

Our results are rather different. All three theoretical models predict zero SH scattering intensity in the forward direction, as well as a small, but finite nonzero, scattering efficiency for particles with a diameter smaller than the wavelength of the fundamental, in clear violation of the physical interpretation given by Wang *et al.* [3]. Furthermore, when we use the gNLRGD$_p$ model to extend the calculation of the scattering parameter $Q_{4\pi}^{2\omega}$ to values of the size parameter larger than 15 (cf. Fig. 8), a maximum in the scattering efficiency is indeed found for $k_m^\omega a \approx 30$. After this maximum, $Q_{4\pi}^{2\omega}$ appears to decay monotonously and asymptotically to its nonzero large-particle limit. No evidence for oscillatory behavior is found. A similar calculation using the NLWKB model does indeed show oscillatory behavior in the curve of $Q_{4\pi}^{2\omega}$ versus $k_m^\omega a$, with maxima for $k_m^\omega a \approx 5$ and 100, respectively, and a minimum for a size parameter of about 50. None of the maxima correspond to a particle size predicted by the model of Wang *et al.* [3]. In NLWKB calculations in which the dispersion was switched off, or in which the refractive indices of the medium were equated to those of the particle, the oscillation disappears. This illustrates that both dispersion and nonequal refractive indices for the medium and the particle are required in order for the scattering efficiency $Q_{4\pi}^{2\omega}$ to develop this oscillatory behavior. Apparently, the phase mismatch between the fundamental and the SH inside the particle does play some role, as predicted by Wang *et al.* [3], but since the medium refractive indices do not enter in their description, their model fails to capture all of the essential physics.

VII. CONCLUSION

We measured the resonance-enhanced surface SHG from a suspension of polystyrene microspheres as a function of particle size in a range of the order of the fundamental wavelength for two different resonance SH-enhancing dyes—MG and Pyr1. Contrary to the case of MG, Pyr1 has not been used in this context before. We found it to behave analogously to MG in all important aspects, except that it possesses a much larger hyperpolarizability. The Pyr1 surface SH signal is not dramatically different from that of the MG adsorbate, which indicates a Pyr1 surface layer of either lower density or with less order than that of the MG layer.

The two dyes gave the same strongly modulated pattern of the forward SH scattering efficiency. Qualitatively similar variations were obtained in calculations based on numerical solution of Maxwell's equations by Pavlyuukh and Hübner [21] and were proposed by them to be an interference effect known from linear Mie scattering (see also [18]). Such resonances would cause large variations in both overall SH scattering efficiency and angular distribution, which could well combine to produce the modulations observed here. Conversely, our measured data provide information that may be essential for solving the issue of the appropriate choice of boundary conditions in nonlinear Mie scattering calculations (cf. [18,21,26,40]).

Direct comparison of the present measurements to the NLRGD and NLWKB model predictions showed that the NLWKB model reproduces well the overall trends in the size dependence but fails with respect to the strong modulations. The standard NLRGD model was found to fail altogether in the particle size range in the experiments, which was well beyond the upper $k_m^\omega a$ value of 0.5 for which the NLRGD and NLWKB models give comparable results. A straightforward generalization of the NLRGD model to allow for dispersion and to use the particle refractive indices instead of those of the surrounding medium improved its applicability range almost an order of magnitude in particle size. The essence of this generalized NLRGD model is that it combines the geometric origins of the SHG contained in the NLRGD theory with those arising from dispersion, first invoked by Wang *et al.* [3], without causing a noteworthy increase in computational efforts.

Our results show that there is an optimal SHG efficiency from dye-coated spherical polystyrene particles in water for $k_m^\omega a \approx 5$, corresponding to a radius similar to the fundamental wavelength inside the particle. To capture the essential features of SHG in this particle size range, one must primarily abandon the optically soft particle approximation and allow for refraction and reflection of the waves at the particle surface. The dispersion of the media plays a negligible role for particles of sizes up to twice the optimal size for SHG. We expect these experimental and theoretical results to be valuable for optimizing experimental parameters, such as particle size and media refractive indices, with respect to the SH collection efficiency.

[1] J. Martorell, R. Vilaseca, and R. Corbalan, in *Quantum Electronics and Laser Science Conference* (Optical Society of America, Washington, DC, 1995), Vol. 16, p. 32.

[2] J. Martorell, R. Vilaseca, R. Corbalan, and J. Trull, in *Photonic Band Gap Materials*, edited by C. Soukoulis (Kluwer, Dordrecht, 1996), p. 529.

[3] H. Wang, E. C. Y. Yan, E. Borguet, and K. B. Eisenthal, Chem. Phys. Lett. **259**, 15 (1996).

[4] K. B. Eisenthal, Chem. Rev. **106**, 1462 (2006).

[5] L. Schneider and W. Peukert, Part. Part. Syst. Charact. **23**, 351 (2006).

[6] H. F. Wang, E. C. Y. Yan, Y. Liu, and K. B. Eisenthal, J. Phys. Chem. B **102**, 4446 (1998).

[7] E. C. Y. Yan, Y. Liu, and K. B. Eisenthal, J. Phys. Chem. B **105**, 8531 (2001).

[8] H. F. Wang, T. Troxler, A. G. Yeh, and H. L. Dai, J. Phys. Chem. C **111**, 8708 (2007).

[9] J. M. Hartings, A. Poon, X. Y. Pu, R. K. Chang, and T. M. Leslie, Chem. Phys. Lett. **281**, 389 (1997).

[10] Y. Liu, E. C. Y. Yan, and K. B. Eisenthal, Biophys. J. **80**, 1004 (2001).

[11] E. C. Y. Yan and K. B. Eisenthal, J. Phys. Chem. B **104**, 6686 (2000).

[12] A. Yamaguchi, M. Nakano, K. Nochi, T. Yamashita, K. Morita, and N. Teramae, Anal. Bioanal. Chem. **386**, 627 (2006).

[13] A. C. Millard, L. Jin, A. Lewis, and L. M. Loew, Opt. Lett. **28**, 1221 (2003).

[14] X. Vidal, A. Fedyanin, A. Molinos-Gómez, S. Rao, J. Martorell, and D. Petrov, Opt. Lett. **33**, 699 (2008).

[15] N. Yang, W. E. Angerer, and A. G. Yodh, Phys. Rev. A **64**, 045801 (2001).

[16] G. Kozyreff, J. L. Dominguez Juarez, and J. Martorell, Phys. Rev. A **77**, 043817 (2008).

[17] A. Molinos-Gomez, M. Maymo, X. Vidal, D. Velasko, J. Martorell, and F. Lopez-Calahorra, Adv. Mater. **19**, 3814 (2007).

[18] J. Dewitz, W. Hübner, and K. H. Bennemann, Z. Phys. D **37**, 75 (1996).

[19] T. Müller, P. H. Vaccaro, F. Balzer, and H. G. Rubahn, Opt. Commun. **135**, 103 (1997).

[20] A. Podlipensky, J. Lange, G. Seifert, H. Graener, and I. Cravetchi, Opt. Lett. **28**, 716 (2003).

[21] Y. Pavlyukh and W. Hübner, Phys. Rev. B **70**, 245434 (2004).

[22] E. V. Makeev and S. E. Skipetrov, Opt. Commun. **224**, 139 (2003).

[23] L. Schneider, H. J. Schmid, and W. Peukert, Appl. Phys. B. **87**, 333 (2007).

[24] J. Martorell, R. Vilaseca, and R. Corbalan, Phys. Rev. A **55**, 4520 (1997).

[25] N. Yang, W. E. Angerer, and A. G. Yodh, Phys. Rev. Lett. **87**, 103902 (2001).

[26] J. I. Dadap, J. Shan, and T. F. Heinz, J. Opt. Soc. Am. B **21**, 1328 (2004).

[27] S. Roke, M. Bonn, and A. V. Petukhov, Phys. Rev. B **70**, 115106 (2004).

[28] J. Shan, J. I. Dadap, I. Stiopkin, G. A. Reider, and T. F. Heinz, Phys. Rev. A **73**, 023819 (2006).

[29] S. H. Jen and H. L. Dai, J. Phys. Chem. B **110**, 23000 (2006).

[30] A. G. F. de Beer and S. Roke, Phys. Rev. B **75**, 245438 (2007).

[31] H. C. van de Hulst, *Light Scattering by Small Particles* (Wiley, New York, 1957).

[32] J. D. Klett and R. A. Sutherland, Appl. Opt. **31**, 373 (1992).

[33] P. N. Butcher and D. Cotter, *The Elements of Nonlinear Optics* (Cambridge University, Cambridge, United Kingdom, 1990).

[34] T. F. Heinz, *Second-Order Nonlinear Optical Effects at Surfaces and Interfaces* (North-Holland, Amsterdam, 1991), Chap. 5.

[35] C. F. Bohren and D. R. Huffman, *Absorption and Scattering of Light by Small Particles* (Wiley, Hoboken, NJ, 1998).

[36] M. I. Mishchenko, *Scattering, Absorption, and Emission of Light by Small Particles* (Cambridge University, Cambridge, United Kingdom, 2002).

[37] G. Arfken, *Mathematical Methods for Physicists* (Academic, San-Diego, CA, 1985).

[38] Polysciences (private communication).

[39] S. Viarbitskaya, V. Kapshai, P. v. d. Meulen, and T. Hansson (unpublished).

[40] S. Viarbitskaya, Ph.D. thesis, Department of Physics, Stockholm University, 2008.

[41] P. Bado, C. Dupuy, K. R. Wilson, R. Boggy, J. Bowen, and S. Westra, Opt. Commun. **46**, 241 (1983).

[42] R. Viajaya, Y. V. G. S. Murti, and T. A. P. Rao, Opt. Quantum Electron. **24**, 575 (1992).

[43] Q. Zhong, Z. Wang, Y. Sun, Q. Zhu, and F. Kong, Chem. Phys. Lett. **248**, 277 (1996).

[44] Y. He, Y. Xiong, Z. Wang, Q. Zhu, and F. Kong, J. Phys. Chem. A **102**, 4266 (1998).

[45] G. A. Reider, A. J. Schmidt, and G. Marowsky, Opt. Commun. **47**, 223 (1983).

[46] F. W. Gordon, S. A. Cresswell, and J. K. Steehler, Langmuir **5**, 286 (1989).

[47] D. L. Akins, C. Akpabli, and X. Li, J. Phys. Chem. **93**, 1977 (1989).

[48] X. Wang, H. Wen, T. He, J. Zuo, C. Xu, and F. C. Liu, Spectrochim. Acta, Part A **53**, 2495 (1997).

[49] K. Clays and B. Coe, Chem. Mater. **15**, 642 (2003).

[50] V. Ostroverkhov, R. G. Petschek, K. D. Singer, and R. J. Twieg, Chem. Phys. Lett. **340**, 109 (2001).

[51] P. Schiebener, J. Straub, J. M. H. Levelt Sengers, and J. S. Gallagher, J. Phys. Chem. Ref. Data **19**, 677 (1990).

[52] X. Ma, J. Q. Lu, R. S. Brock, K. M. Jacobs, P. Yang, and X. H. Hu, Phys. Med. Biol. **48**, 4165 (2008).

[53] J. I. Dadap, J. Shan, K. B. Eisenthal, and T. F. Heinz, Phys. Rev. Lett. **83**, 4045 (1999).

[54] H. M. Eckenrode, S. H. Jen, J. Han, A. G. Yeh, and H. L. Dai, J. Phys. Chem. B **109**, 4646 (2005).

[55] Y. Zhao and L. Ma, Appl. Opt. **48**, 591 (2009).